






Pulmonary lesions following inoculation with the SARS-CoV-2 Omicron BA.1 (B.1.1.529) variant in Syrian golden hamsters

Melanie Rissmann, Danny Noack, Debby van Riel, Katharina S. Schmitz, Rory D. de Vries, Peter van Run , Mart M. Lamers , Corine H. Geurts van Kessel, Marion P. G. Koopmans , Ron A. M. Fouchier, Thijs Kuiken, Bart L. Haagmans  and Barry Rockx 

Department of Viroscience, Erasmus Medical Center, Rotterdam, Netherlands

ABSTRACT

The Omicron BA.1 (B.1.1.529) SARS-CoV-2 variant is characterized by a high number of mutations in the viral genome, associated with immune escape and increased viral spread. It remains unclear whether milder COVID-19 disease progression observed after infection with Omicron BA.1 in humans is due to reduced pathogenicity of the virus or due to pre-existing immunity from vaccination or previous infection. Here, we inoculated hamsters with Omicron BA.1 to evaluate pathogenicity and kinetics of viral shedding, compared to Delta (B.1.617.2) and to animals re-challenged with Omicron BA.1 after previous SARS-CoV-2 614G infection. Omicron BA.1 infected animals showed reduced clinical signs, pathological changes, and viral shedding, compared to Delta-infected animals, but still showed gross- and histopathological evidence of pneumonia. Pre-existing immunity reduced viral shedding and protected against pneumonia. Our data indicate that the observed decrease of disease severity is in part due to intrinsic properties of the Omicron BA.1 variant.

ARTICLE HISTORY Received 12 May 2022; Revised 20 June 2022; Accepted 26 June 2022

KEYWORDS SARS-CoV-2; Omicron BA.1; Delta; Syrian golden hamster; pathology; re-challenge; pre-existing immunity



Introduction


On 31st December 2019, the World Health Organization (WHO) was informed of a cluster of cases of pneumonia of unknown cause detected in Wuhan City, Hubei Province of China. A novel coronavirus (SARS-CoV-2) was identified [1]. Characterized by high transmissibility, this novel disease named coronavirus disease 2019 (COVID-19) rapidly spread throughout the whole world. As of 9 March 2022, WHO has reported almost 440 million SARS-CoV-2 infections with over 6 million confirmed deaths worldwide [2]. The WHO has been monitoring and assessing the evolution of SARS-CoV-2 since its emergence and designated specific Variants of Concern (VOCs) that pose an increased risk to global public health. To date, several VOCs of SARS-CoV-2 have been identified with sets of mutations in the spike protein or other sites in the viral genome, linked to increased transmission or disease, or evasion of immune responses [3].

The VOC Omicron BA.1 (B.1.1.529) was initially reported in South Africa and Botswana in November 2021 [4], but has spread rapidly and is the predominant strain replacing the previously dominant Delta strain (B.1.617.2) in many countries worldwide.

A striking feature of this variant is that it has an unusual large number of mutations in the spike protein, leading to partial evasion of pre-existing antibodies, and rendering it unsusceptible to the majority of monoclonal antibody therapies approved for clinical use [5–7]. In addition, epidemiological data suggest that infection with the Omicron BA.1 variant leads to less severe disease in humans [8], although it remains unknown whether this decrease in pathogenicity is primarily caused by intrinsic properties of the virus or if the observed milder course of disease in humans is due to pre-existing immunity, either from vaccination or previous exposure to other SARS-CoV-2 variants [9]. A variant dependent decrease of disease severity was supported by first observations of limited pathogenicity of Omicron BA.1 in immunologically naïve Syrian golden hamsters [10,11].

To evaluate the intrinsic pathogenic potential of the emerging Omicron BA.1 variant, groups of Syrian golden hamsters were infected with Omicron BA.1. Results were compared to hamsters infected with the Delta variant. In addition, we evaluated whether previous exposure to the ancestral SARS-CoV-2 strain 614G affords protection against heterologous challenge with the antigenically distinct Omicron BA.1 variant.

CONTACT Bart L. Haagmans  b.rockx@erasmusmc.nl; Barry Rockx  b.haagmans@erasmusmc.nl

 Supplemental data for this article can be accessed online at <https://doi.org/10.1080/22221751.2022.2095932>.

© 2022 The Author(s). Published by Informa UK Limited, trading as Taylor & Francis Group, on behalf of Shanghai Shangyixun Cultural Communication Co., Ltd. This is an Open Access article distributed under the terms of the Creative Commons Attribution License (<http://creativecommons.org/licenses/by/4.0/>), which permits unrestricted use, distribution, and reproduction in any medium, provided the original work is properly cited.

Methods

Viruses and cells

Calu-3 cells were cultured in Opti-MEM I (1) + GlutaMAX (Gibco) supplemented with 10% FBS, penicillin (100 IU/mL), and streptomycin (100 IU/mL) at 37°C in a humidified CO₂ incubator. Cells were tested negative for mycoplasma. Bavpat-1 (614G), Delta (B.1.617.2) and Omicron BA.1 (B.1.1.529) variants of SARS-CoV-2 were propagated as described before [12]. Briefly, all used viruses were propagated to passage 3 on Calu-3 (ATCC HTB-55) cells in Advanced DMEM/F12 (Gibco), supplemented with HEPES, Glutamax, penicillin (100 IU/mL) and streptomycin (100 IU/mL) (AddDF+++) at 37°C in a humidified CO₂ incubator. Infections were performed at a multiplicity of infection (MOI) of 0.01 and virus was harvested after 72 h. The culture supernatant was cleared by centrifugation at 1000 × g for 5 min and stored at -80°C in aliquots. Virus titres were determined by plaque assay as described below. The Delta and Omicron BA.1 sequences are available on GenBank under accession numbers OM287123 and OM287553, respectively. All work with infectious SARS-CoV-2 was performed in a Class II Biosafety Cabinet under BSL-3 conditions at Erasmus Medical Center.

Animals and experimental setup

Female Syrian golden hamsters (*Mesocricetus auratus*; 6 weeks old; Janvier, France) were handled in an ABSL-3 biocontainment laboratory (Supplementary material). Groups of animals ($n = 8$) were inoculated intranasally with 5×10^4 PFU of the Omicron BA.1 or Delta variants of SARS-CoV-2 or PBS (mock; $n = 4$) in a total volume of 100 µl per animal. Throat swabs and nasal washes (250 µL) were taken at 1, 3, 5, 7, 10, 14, 18 and 21 days post inoculation (dpi). The body weight of animals was measured daily for the first 10 days of the experiment and at all days of sampling thereafter. On 5 dpi, animals ($n = 4$) from one group of each variant were euthanized and the respiratory tract (nasal turbinate, trachea and lungs) was sampled for quantification of viral and genomic load, as well as for histopathology and virus antigen expression. All remaining animals were sacrificed 26 dpi.

A single group of hamsters ($n = 4$) previously inoculated intranasally with 10^3 TCID₅₀ of Bavpat-1 (isolate BetaCoV/Munich/BavPat1/2020; European Virus Archive Global #026 V 03883; kindly provided by Dr. C. Drosten) was challenged at 13 dpi by intranasal inoculation with 5×10^4 PFU Omicron BA.1 in a volume of 100 µl. Throat swabs were taken at 1, 3 and 5 dpi and the animals were weighed daily. All animals of this group were sacrificed at 5 dpi.

RNA extraction and genome quantification with RT-qPCR

All throat swabs, nasal washes and tissue samples were used for RNA extraction and following quantification of SARS-CoV-2 genome by RT-qPCR. RNA extraction was performed as described previously [13]. A RT-qPCR targeting the E gene of SARS-CoV-2 was used as previously reported [14]. Ct values were compared to a standard curve derived from a titrated 614G virus stock.

Plaque assay

All throat swabs, nasal washes and tissue samples that were taken post mortem at 5 dpi were used for quantification of viral loads via a plaque assay on Calu-3 cells as described before [15]. Briefly, ten-fold serial diluted samples were added to monolayers of Calu-3 cells. Cells were incubated with inoculums at 37°C for 4 h, washed once with PBS and then overlaid with 1.2% Avicel (FMC biopolymers) in Opti-MEM I (1X) + GlutaMAX for two days. Cells were fixed in 4% formalin for 20 min, permeabilized in 70% ice-cold ethanol and washed in PBS. Cells were blocked in 3% BSA (bovine serum albumin; Sigma) in PBS and stained with rabbit anti-nucleocapsid (Sino biological; 1:2000) in PBS containing 0.1% BSA, washed thrice, and stained with donkey anti-rabbit Alexa Fluor 488 (Invitrogen; 1:4000) in PBS containing 0.1% BSA. Plates were washed and scanned on the Amersham Typhoon Biomolecular Imager (channel Cy2; resolution 25 µm; GE Healthcare). All staining steps were performed at room temperature for one hour. Plaque assay analysis was performed using ImageQuant TL 8.2 software (GE Healthcare).

Plaque reduction neutralization assay

Plaque reduction neutralization assays were performed as described previously [12]. Briefly, heat-inactivated sera were two-fold diluted in OptiMEM medium starting at a dilution of 1:10 in 60 ul. 400 plaque forming units of SARS-CoV-2 614G were added to each well in 60ul of virus suspension incubated at 37°C for 1 h. After 1 h of incubation, the virus-antibody mixtures were transferred onto Calu-3 cells and were incubated for 8 h at 37°C. After incubation, cells were fixed and plaques were stained with monoclonal mouse anti-SARS-CoV-2 nucleocapsid antibody (Sino Biological) and a secondary peroxidase-labeled goat anti-mouse IgG (Dako). Nuclei were stained with Hoechst for 30 min. Cells were imaged using the Opera phenix spinning disk confocal HCS system as described before [16].

Histopathology and immunohistochemistry

Nasal turbinates, trachea and lungs were fixed in 4% neutral-buffered formalin, embedded in paraffin, and sectioned at 4 μ m. Sections of all tissue samples were stained with haematoxylin and eosin for histopathological analysis, and consecutive sections were stained by immunohistochemistry for SARS-CoV-2 antigen expression, as described previously [17].

Statistical analysis

All statistical analyses were performed using GraphPad Prism 9 software (La Jolla, CA, USA). Applied tests are indicated in according figure legends.

Results

Clinical manifestation and shedding after inoculation of Syrian golden hamsters with Omicron BA.1 or Delta

Following intranasal inoculation of Syrian golden hamsters with the Omicron BA.1 and Delta variants of SARS-CoV-2, differences in clinical manifestation were monitored by body weight measurements of individual animals (Figure 1(A)). Compared to mock-infected hamsters, infection with the Delta variant resulted in a significant body weight loss of maximum 14%, peaking at 4–5 dpi. No weight loss was observed in animals infected with the Omicron BA.1 variant and animals gained weight comparable to mock-infected animals.

To evaluate if Omicron BA.1 and Delta variants were shed to a varying extent via the upper respiratory tract, both nasal washes and throat swabs were taken regularly throughout the experiment. SARS-CoV-2 genome was detected in the nasal wash and throat swabs of all hamsters until 21 dpi (Figure 1(B,C)). Occasionally, significant differences in detection of genomic RNA between Omicron BA.1 and Delta were observed, that were confirmed by the comparison of cumulative shedding (Figure 1(D,E)). In nasal washes, infectious virus was only found up to 3 dpi (Figure 1(F)). Significantly lower amounts of infectious virus were detected in the nasal washes of Omicron BA.1 infected animals on 1 dpi, compared to animals infected with Delta ($p < 0.0001$). Infectious virus in throat swabs was only detectable on 1 dpi, with no significant differences between the two groups (Figure 1(G)).

Pathogenesis of Omicron BA.1 infection in the Syrian golden hamster

Despite the fact that Omicron BA.1 infected animals did not show weight loss, gross postmortem examination at 5 dpi revealed single or multiple foci of

pulmonary consolidation, visible as well-delimited, slightly raised, dark red areas, covering 50–90% of the lung surface (Figure 2(A)). Due to animal-to-animal variation, no clear differences in pulmonary consolidation were observed between Delta and Omicron BA.1. A significant difference in the percentage of inflamed lung area was observed, with an average of 78% of the lung area affected in Delta variant infected animals, compared to 38% in Omicron BA.1 infected animals (Figure 2(B), Supplemental Figure S1A,C). No significant difference in the amount of viral antigen expression was observed between Omicron BA.1 and Delta (Figure 2(C)). The main histopathological changes in the lungs of both Omicron BA.1 and Delta infected animals were multiple areas of diffuse alveolar damage, characterized by flooding of alveolar lumina by variable proportions of neutrophils and macrophages, mixed with fibrin and oedema fluid; and by type II pneumocyte hyperplasia (Figure 2(D,H)). By immunohistochemistry, mainly type I pneumocytes at the edges of the lesions expressed viral antigen with less than 2% of the lung area being positive (Figure 2(E,I), Supplemental Figure S1B,D).

The main histopathological changes in the nasal turbinates of both Omicron BA.1 and Delta infected animals were necrosis and inflammation of the olfactory mucosa. This was characterized by the presence of many neutrophils mixed with cellular debris and fibrin in the lumina of the nasal turbinates, as well as infiltration with variable numbers of neutrophils in the underlying olfactory mucosa (Figure 2(E,J)). In addition, there was multifocal attenuation of the olfactory mucosa, indicative of previous loss of epithelial cells due to infection at earlier time points. Both the amount of neutrophil infiltration and of olfactory mucosal attenuation appeared to be increased in Delta-infected animals than in Omicron BA.1-infected animals. SARS-CoV-2 antigen was mainly found in cellular debris within the lumina of nasal turbinates, again indicative of damage at earlier timepoint. Additionally, small foci within the olfactory mucosa were found to be positive for viral antigen (Figure 2(G,K)). Furthermore, respiratory epithelial cells were occasionally found to carry viral antigen in Delta, but not Omicron BA.1 infected animals. There were no clear differences in the amount of virus antigen expression between Omicron BA.1- and Delta-infected animals. Neither virus antigen expression nor lesions were found in the tracheas of any of the animals.

SARS-CoV-2 in respiratory tissues of Omicron BA.1 infected Syrian golden hamsters

Besides of pulmonary lesions and the presence of viral antigen, respiratory tissue was also evaluated for the presence of viral RNA via RT-qPCR and infectious

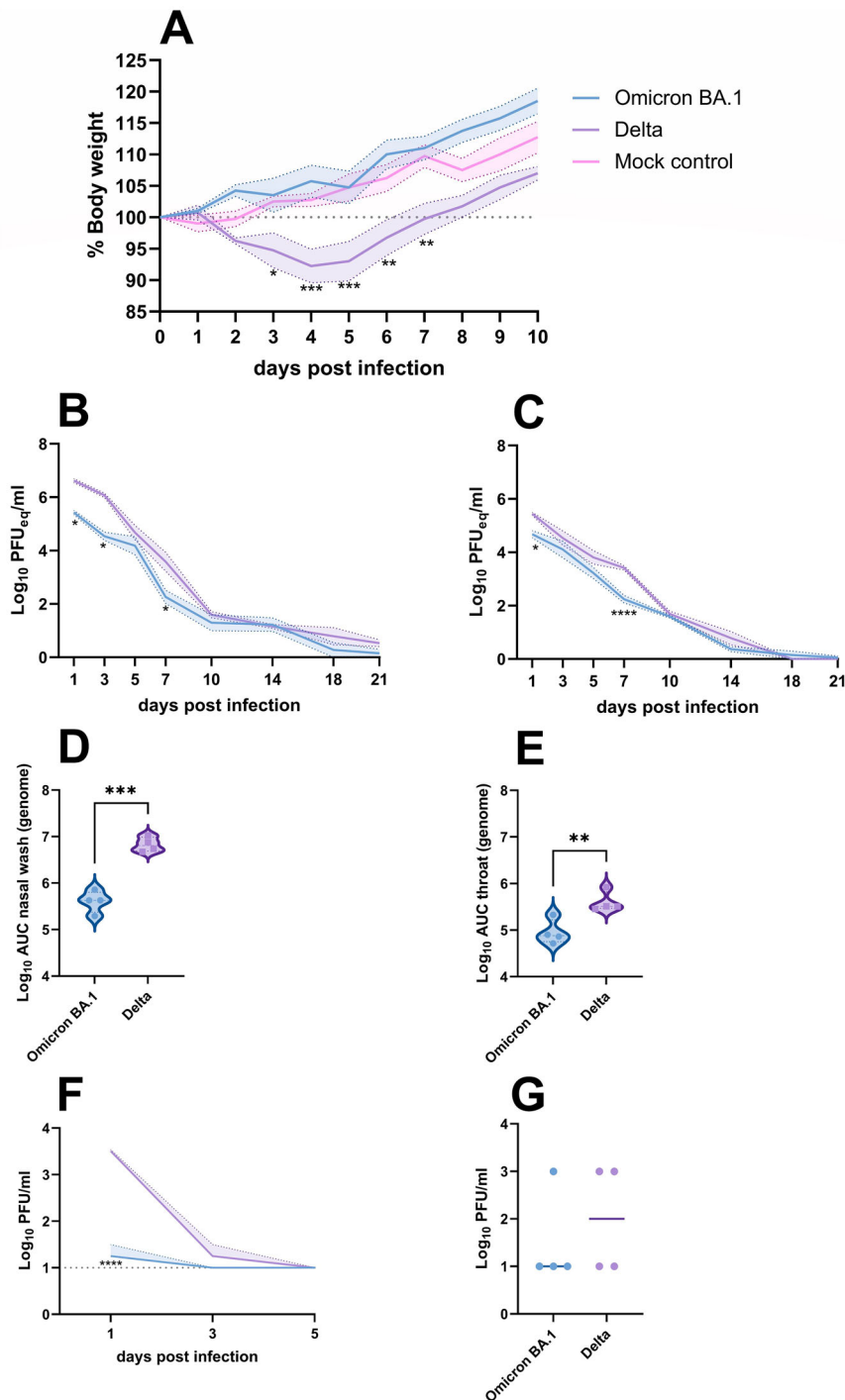


Figure 1. Clinical manifestation and shedding after Omicron BA.1 and Delta inoculation. (A) Relative body weight of hamsters inoculated with Omicron BA.1, Delta and mock-inoculated hamsters. The mean of each group is shown as solid line, SEM displayed as shading. Significant statistical differences between the three groups were calculated with a 2-way ANOVA with Tukey's multiple comparison test. Significant differences to the mock control are indicated with * ($p < 0.05$; ** $p < 0.01$; *** $p < 0.001$). (B,C) Kinetics of respiratory shedding detected in (B) nasal washes and (C) throat swabs. The mean of each group is shown as solid line, SEM displayed as shading. Significant statistical differences (* $p < 0.05$; **** $p < 0.0001$) were calculated with 2-way ANOVA with Dunnett's correction for multiple comparisons. (D,E) Cumulative shedding depicted as area under the curve (AUC) in (D) nasal washes and (E) throat swabs. Significant statistical differences were calculated with unpaired t-test (** $p < 0.01$; *** $p < 0.001$). (F,G) Detection of infectious virus. (F) Infectious virus in nasal washes. The mean of each group is shown as solid line, SEM displayed as shading. Significant statistical differences (**** $p < 0.0001$) were calculated with 2-way ANOVA with Dunnett's correction for multiple comparisons. (G) Infectious virus in throat swabs at 1 dpi. The mean of each group is depicted as horizontal line. Significant statistical differences were calculated with unpaired t-test.

virus. SARS-CoV-2 genome copies were lower in respiratory tissues of Omicron BA.1 inoculated hamsters, compared to hamsters infected with the Delta variant. However, statistically significant differences were only

detected in the nasal turbinates when compared to Delta infected animals (Figure 3(A)). Infectious virus was mainly found in the nasal turbinates, although low virus titres were also found in the lungs of one

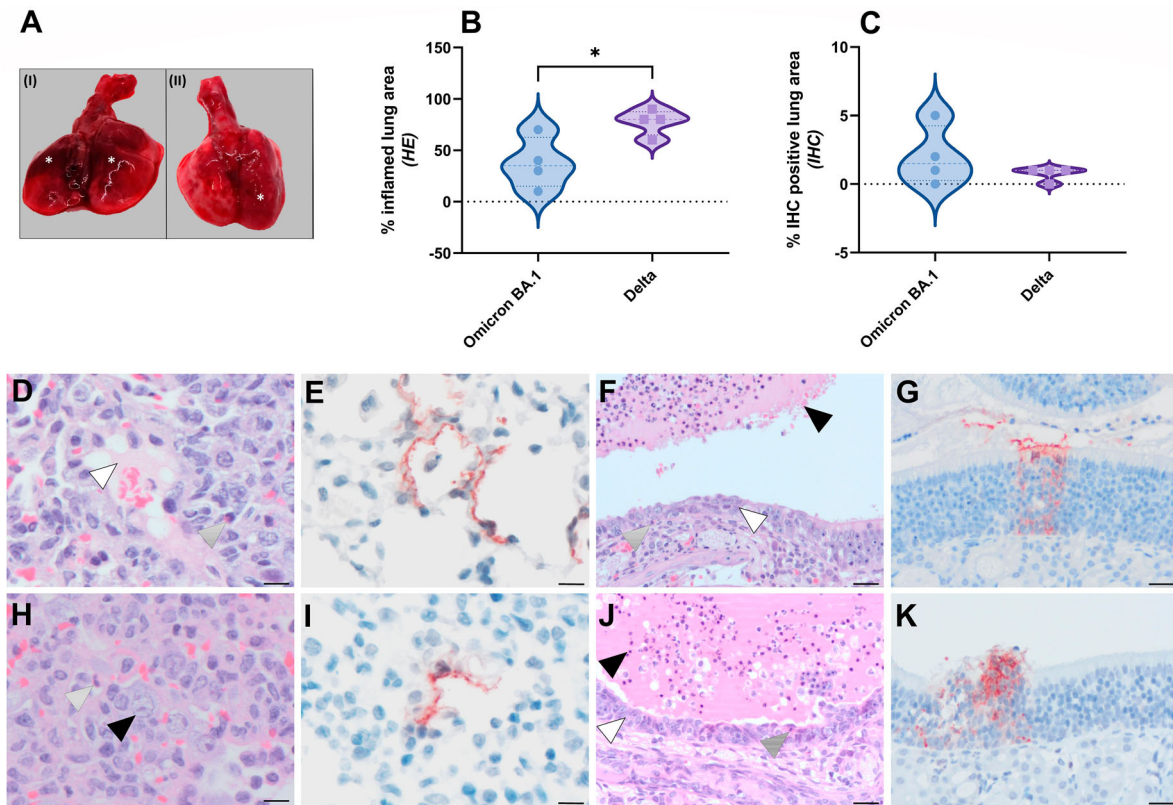


Figure 2. Pathological lesion and quantitative scoring of histopathological changes and viral antigen expression in Omicron BA.1 or Delta inoculated hamsters. (A) Representative gross pathological lesions of animals inoculated with (I) Omicron BA.1 or (II) Delta. Foci (*) of pulmonary consolidation. (B) Percentage of inflamed lung areas detected in HE staining and (C) % of viral antigen-positive lung areas detected in IHC. Significant statistical differences between two groups were calculated with unpaired *t*-test (* $p < 0.05$). (D–K) Histopathological changes and viral antigen expression in nasal turbinates and lungs of Omicron BA.1 and Delta inoculated hamsters. (D) H&E staining and (E) IHC of lungs of Syrian golden hamsters, infected with Omicron BA.1. (F) H&E staining and (G) IHC of nasal turbinates of Syrian golden hamsters, infected with Omicron BA.1. (H) H&E staining and (I) IHC of lungs of Syrian golden hamsters, infected with Delta. (J) H&E staining and (K) IHC of nasal turbinates of Syrian golden hamsters, infected with Delta. Bars indicate 20 μ m. (D,H) Proportions of neutrophils (*striped arrowheads*), oedema fluid (*white arrowhead*) and type II pneumocyte hyperplasia (*black arrowhead*) can be found in lungs of Omicron BA.1 and Delta inoculated hamsters. (F,J) The nasal turbinates of both Omicron BA.1 and Delta infected animals were characterized by the presence of many neutrophils mixed with cellular debris and fibrin in the lumina of the nasal turbinates (*black arrowhead*), infiltration with variable numbers of neutrophils in the underlying olfactory mucosa (*striped arrowhead*) and multifocal attenuation of the olfactory mucosa (*white arrowhead*).

out of four Omicron BA.1 and one out of four Delta infected hamsters (Figure 3(B)). No infectious virus was found in the trachea.

Protective effect of previous inoculation with 614G SARS-CoV-2 on re-challenge with Omicron BA.1

Animals that were inoculated with SARS-CoV-2 614G were found to shed viral genome via the upper respiratory tract, peaking from 1 to 4 dpi. At the day of re-challenge, only limited viral genome was detected in all animals (Figure 4(A)). All hamsters had neutralizing antibody responses after initial infection (antibody neutralization titres of 1:2024; 1:2489; 1:2090; 1:1766). Following heterologous re-challenge, no changes in the percentage of body weight were observed (Figure 4(B)). At 3 and 5 dpi, significantly less SARS-CoV-2 genome was detected in throat swabs of re-challenged

animals ($p < 0.0001$) compared to Omicron BA.1 infected hamsters (Figure 4(C)). No infectious virus was detected in any throat swabs of the re-challenged animals. No gross lesions were observed in the lungs of re-challenged animals (Figure 4(D)).

The genomic viral burden in nasal turbinates, trachea and lungs was significantly higher in naïve hamsters infected with Omicron BA.1, compared to re-challenged animals. This difference was most pronounced in the lungs ($p = 0.0004$) (Figure 4(E)). No infectious virus was found in any tissue of re-challenged animals. No histopathological changes or viral antigen expression were found in the lungs or nasal turbinates of re-challenged hamsters (Figure 4(F–I)).

Discussion

Following the identification of SARS-CoV-2 as the cause of coronavirus disease-2019 (COVID-19), the

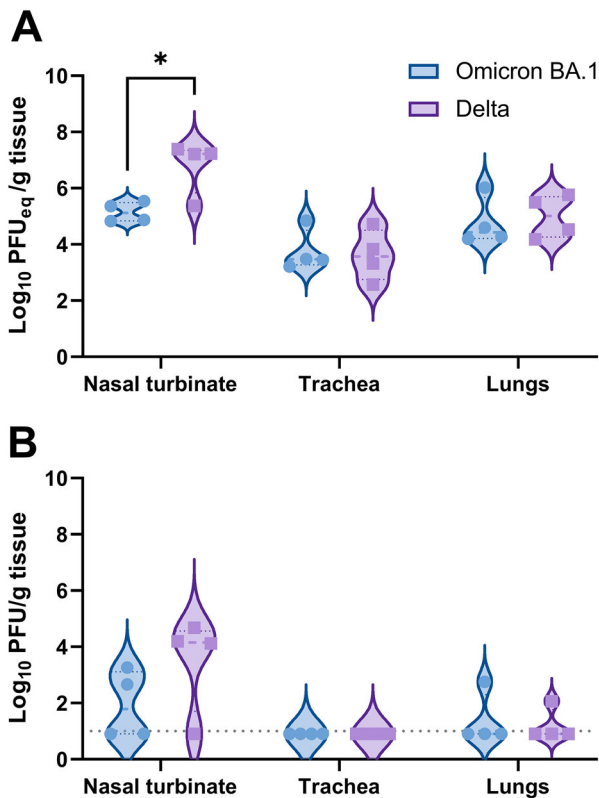


Figure 3. Detection of SARS-CoV-2 in respiratory tissue of Omicron BA.1 or Delta inoculated hamsters. (A) Detection of SARS-CoV-2 genome in respiratory tissue of inoculated hamsters. Significant statistical differences were calculated with unpaired *t*-test ($*p < 0.05$). (B) Detection of infectious virus in respiratory tissue of Omicron BA.1 and Delta infected Syrian golden hamsters. Significant statistical differences were calculated with unpaired *t*-test.

virus has spread rapidly throughout the world. Since its emergence, viral genomic sequence analysis has allowed tracking of the emergence of SARS-CoV-2 variants. While many of the observed mutations in the SARS-CoV-2 genome are neutral, or deleterious, some mutations are associated with an increase of viral fitness. These changes may include immune escape as well as changes in pathogenicity, infectivity and transmissibility [3].

This study shows that in the hamster model, the recently emerged VOC Omicron BA.1, does not cause body weight loss but still induces gross- and histopathological changes in the upper and lower respiratory tract with decreased viral shedding compared to the Delta variant of SARS-CoV-2. However, a previous inoculation with the ancestral 614G SARS-CoV-2 confers complete protection from pneumonia or viral replication in the respiratory tract.

As shown by us and others, inoculation of hamsters with ancestral SARS-CoV-2 614G results in significant but transient body weight loss peaking at 4–5 dpi in the absence of overt respiratory signs, making body weight loss a valuable readout for clinical impact of SARS-CoV-2 inoculation [18]. Here, we show that the Delta variant causes significant body weight loss

in hamsters, whereas no weight loss can be observed after infection with Omicron BA.1 in a direct comparison. Although most other studies observed a limited body weight loss or at least decreased weight gain compared to non-infected animals, a marked reduction of disease severity after infection with Omicron BA.1 is reported throughout all previous studies [10,11], similar to what is observed in humans [19].

Previous studies in clinical settings have shown that viral genome of certain SARS-CoV-2 variants is shed at higher levels than for other variants. This increased shedding in part has been suggested to contribute in the increased spread of these variants [20]. However, recent analysis of human specimens are indicative of no major differences in shedding between the SARS-CoV-2 variants Delta and Omicron BA.1 [21]. We demonstrated that the kinetics of viral genome shedding were not significantly different between Delta and Omicron BA.1 infected hamsters. Different from previous reports of other groups, where Omicron BA.1 RNA was only shed until 9 dpi and Delta until 12 dpi [22], we observed shedding until 21 dpi. Recent studies also demonstrated that the transmissibility in a non-contact transmission setup is increased for Omicron infected animals compared to Delta infected animals. Both groups had comparable titres in nasal turbinates of index animals with lower viral shedding in Omicron BA.1 infected animals during the course of infection [22]. Collectively, this indicates that evaluation of viral shedding in the hamster model cannot solely elucidate the transmissibility of different VOCs.

While no body weight loss was observed in Omicron BA.1 infected animals, these animals still showed diffuse alveolar damage and viral antigen expression, although milder compared to infection with Delta and to previously reported inoculation with the ancestral 614G strain [23]. This observation stands in contrast to previous reports of Omicron BA.1 infections in hamsters, describing limited or no inflammation in the lower respiratory tract [10,11,22]. A lower inoculation dose of 10^3 PFU in 50 μ l, compared to 5.0×10^4 PFU in 100 μ l used in this study, may explain the differences for one previous study [3]. However, two other studies used even higher doses of 10^5 PFU in 100 μ l [12] or 10^5 PFU in 30 μ l [4] and only saw limited pathology. In these studies, viral stocks were prepared on Vero-TMPRSS2 cells. Upon passaging in Vero cells that lack TMPRSS2, SARS-CoV-2 may rapidly acquire multibasic cleavage site mutations that diminish S1/S2 cleavage, which leads to ineffective TMPRSS2-mediated entry into airway cells and decreased replication in hamsters [24–27]. Vero cells stably expressing TMPRSS2 can also be used for this purpose [25], but Omicron grown on these cells also shows a reduced S1/S2 cleavage of the spike protein compared with Delta [28]. In contrast, when we grew viruses on the TMPRSS2-expressing Calu-3

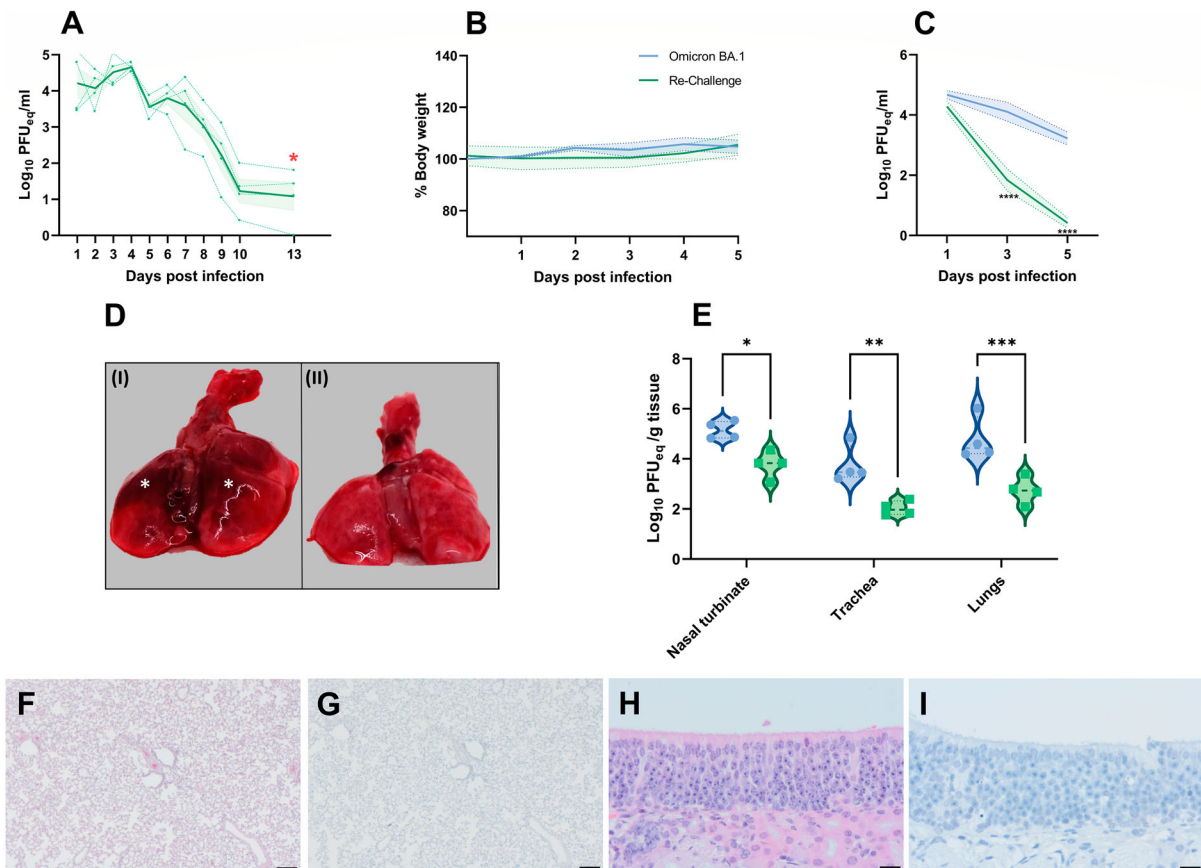


Figure 4. Effect of Omicron BA.1 re-infection in 614G convalescent Syrian golden hamsters. (A) Detection of viral genome in throat swabs of 614G infected Syrian golden hamsters prior to re-challenge. The mean of each group is shown as solid line, SEM displayed as shading. Data of individual animals is depicted as dashed line. Time point of re-challenge with Omicron BA.1 (13 dpi) is indicated with a red star. (B) Relative body weight of immunologically naïve hamsters infected with Omicron and convalescent hamsters re-challenged with Omicron BA.1. The mean of each group is shown as solid line, SEM displayed as shading. Significant statistic differences were calculated with 2-way ANOVA with Dunnett's correction for multiple comparisons. (C) Detection of viral genome in throat swabs of immunologically naïve hamsters infected with Omicron BA.1 and convalescent hamsters re-challenged with Omicron. The mean of each group is shown as solid line, SEM displayed as shading. Significant statistic differences ($****p < 0.0001$) were calculated with 2-way ANOVA with Dunnett's correction for multiple comparisons. (D) Representative gross pathological lesions of animals inoculated with (I) Omicron BA.1¹ or (II) 614G convalescent and Omicron BA.1 re-challenged animals. Foci (*) of pulmonary consolidation. (E) Detection of SARS-CoV-2 genome² in respiratory tissue of infected hamsters. Significant statistic differences were calculated with unpaired *t*-test (*: $p < 0.05$). (F-I) Histopathological changes and viral antigen expression in nasal turbinates and lungs of re-challenged Syrian golden hamsters. (F) H&E staining and (G) IHC of lungs. (H) H&E staining and (I) IHC of nasal turbinates. Bars indicate 200 μ m for images of the lungs and 20 μ m for the nasal turbinates. ^{1,2} Data shown for comparison to Omicron BA.1 inoculated hamsters are based on data shown in Figure 1 (¹) and Figure 3 (²).

cells to prevent cell culture adaptation, a proper cleavage of the spike protein was observed [25]. Thus, the Omicron BA.1 virus used in our study – when passaged on Calu-3 cells – showed a fully cleaved spike protein [29]. In line with earlier findings, these findings suggest that the S1/S2 cleavage may determine replication and pathogenicity of SARS-CoV-2 variants including Omicron in vivo, but future follow up experiments are needed to further explore this.

Furthermore, although looking at different time points post inoculation, a recent study also found that the replication and pathogenicity of Omicron BA.2 is comparable to that of BA.1 in rodents, highlighting the existent, but significantly reduced pathogenesis of newly emerged Omicron variants [30].

A hypothesis for the observed decrease in pathogenesis is that the heavily mutated RBD of Omicron

BA.1 has a decreased affinity to hamster ACE-2 and is much better adapted to human ACE-2. Studies using hACE2 transgenic mice [11] showed a less severe course of Omicron BA.1 infection in those animals, compared to ancestral strains or previous VOCs. Although this does highlight that a change of binding affinity to species-specific ACE-2 cannot explain the observed differences in pathogenicity, a recent publication found a reduced predicted interaction enhancement of the Spike protein of Omicron with the ACE-2 of Syrian golden hamsters when compared to humans [31]. Thus, the specific role of changes in binding affinity of the RBD of emerging SARS-CoV-2 variants with species-specific ACE-2 should be investigated in perspective studies.

While the observed reduction in disease severity in humans may (in part) be the result of intrinsic

properties of the virus, the presence of pre-existing immunity, due to vaccination or previous infection, may also affect the disease outcome. We previously showed that the Omicron BA.1 variant is antigenically distinct from the other SARS-CoV-2 variants [16], and several studies have shown that neutralizing monoclonal antibodies against the ancestral SARS-CoV-2 strain have limited neutralizing capacity against the Omicron BA.1. Although a recent study has proven that hamsters with a heterologous re-challenge are protected from B.1.1.7 (Alpha) and B.1.351 (Beta) induced acute pneumonia, already 14 days after initial infection, the cross-protective potential towards Omicron BA.1 was not investigated [32]. Interestingly, despite the antigenic distance and early time point for re-infection, the 614G convalescent group was completely protected from any pathological alterations of the respiratory tract after infection with Omicron BA.1. This indicates a strong cross-protective effect of heterologous re-infections and will need further investigations of the mechanistic background and scope of this cross-protection in prospective studies. Additionally, the experimental setup of re-challenge of convalescent animals can be a useful tool to study if observed decrease in disease severity is mainly driven by viral factors or pre-existing immunity.

In conclusion, with the continuing emergence of SARS-CoV-2 variants, models to evaluate potential phenotypic changes associated with mutations are invaluable in assessing the impact on public health. In hamsters, the currently circulating dominant SARS-CoV-2 Omicron BA.1 variant, shows reduced viral shedding and disease, recapitulating the phenotype seen in human cases. Interestingly, remaining pathogenicity in the lower respiratory tract can still be detected without being reflected in clinical manifestation. In summary, we show that the hamster model remains useful in assessing the impact of SARS-CoV-2 variants on disease severity and the role of pre-existing immunity. Thus, the model continues to be an important tool in the evaluation of pathogenicity of different SARS-CoV-2 variants and studying the efficacy of intervention strategies.

Acknowledgements

We thank J.M. Fentener van Vlissingen, Ingeborg van Middelkoop, Rianne Stam, Vincent Duiverman and Vincent Vaes for assistance with the animal studies.

Disclosure statement

No potential conflict of interest was reported by the author(s).

Funding

This research is (partly) financed by the NWO Stevin Prize awarded to M.P.G.K. by the Netherlands Organisation for Scientific Research (NWO), and B.L.H., R.A.M.F., B.R., and M.P.G. are supported by the NIH/NIAID Centers of Excellence for Influenza Research and Response (CEIRR) under contract 75N93021C00014-Icahn School of Medicine at Mt. Sinai.

Author contributions

Conceptualization, B.R., M.R., R.F. B.H.; investigation, M.R., D.N., D.v.R., K.S.S., R.D.d.V., P.v.R., T.K. and B.R.; resources, M.L., C.G.v.K., M.P.G.K.; supervision, B.R., R.D.d.V and B.H.; writing, original draft, B.R., M.R., and B.H.; writing–review and editing, all authors; funding acquisition: M.P.G.K., R.F. B.H., B.R.,

Data and materials availability

Viruses must be obtained through an MTA.

ORCID

Peter van Run  <http://orcid.org/0000-0001-6963-4165>

Mart M. Lamers  <http://orcid.org/0000-0002-1431-4022>

Marion P. G. Koopmans  <http://orcid.org/0000-0002-5204-2312>

Bart L. Haagmans  <http://orcid.org/0000-0001-6221-2015>

Barry Rockx  <http://orcid.org/0000-0003-2463-027X>

References

- [1] Zhu N, Zhang D, Wang W, et al. A novel coronavirus from patients with Pneumonia in China, 2019. *N Engl J Med.* 2020 Feb 20;382(8):727–733.
- [2] WHO COVID-19 Dashboard. Geneva: World Health Organization. 2022; Available from: <https://covid19.who.int/>.
- [3] Plante JA, Mitchell BM, Plante KS, et al. The variant gambit: COVID-19's next move. *Cell Host Microbe.* 2021 Apr 14;29(4):508–515.
- [4] Petersen E, Ntoumi F, Hui DS, et al. Emergence of new SARS-CoV-2 variant of concern Omicron (B.1.1.529) – highlights Africa's research capabilities, but exposes major knowledge gaps, inequities of vaccine distribution, inadequacies in global COVID-19 response and control efforts. *Int J Infect Dis.* 2022 Jan;114:268–272.
- [5] Callaway E. Heavily mutated Omicron variant puts scientists on alert. *Nature.* 2021 Dec;600(7887):21–21.
- [6] Chen J, Wang R, Gilby NB, et al. Omicron variant (B.1.1.529): infectivity, vaccine breakthrough, and antibody resistance. *J Chem Inf Model.* 2022 Jan 24;62(2):412–422.
- [7] VanBlargan LA, Errico JM, Halfmann PJ, et al. An infectious SARS-CoV-2 B.1.1.529 Omicron virus escapes neutralization by therapeutic monoclonal antibodies. *Nat Med.* 2022 Mar;28(3):490–495.
- [8] Wolter N, Jassat W, Walaza S, et al. Early assessment of the clinical severity of the SARS-CoV-2 omicron

- variant in South Africa: a data linkage study. *Lancet*. 2022 Jan 29;399(10323):437–446.
- [9] Sigal A. Milder disease with Omicron: is it the virus or the pre-existing immunity? *Nat Rev Immunol*. 2022 Feb;22(2):69–71.
- [10] Abdelnabi R, Foo CS, Zhang X, et al. The omicron (B.1.1.529) SARS-CoV-2 variant of concern does not readily infect Syrian hamsters. *Antiviral Res*. 2022 Jan 21;198:105253.
- [11] Halfmann PJ, Iida S, Iwatsuki-Horimoto K, et al. SARS-CoV-2 Omicron virus causes attenuated disease in mice and hamsters. *Nature*. 2022 Mar;603(7902):687–692.
- [12] GeurtsvanKessel CH, Geers D, Schmitz KS, et al. Divergent SARS CoV-2 Omicron-reactive T- and B cell responses in COVID-19 vaccine recipients. *Sci Immunol*. 2022 Mar 25;7(69):eabo2202.
- [13] de Vries RD, Schmitz KS, Bovier FT, et al. Intranasal fusion inhibitory lipopeptide prevents direct-contact SARS-CoV-2 transmission in ferrets. *Science*. 2021 Mar 26;371(6536):1379–1382.
- [14] Corman VM, Landt O, Kaiser M, et al. Detection of 2019 novel coronavirus (2019-nCoV) by real-time RT-PCR. *Euro Surveill*. 2020 Jan;25(3):2000045.
- [15] Lamers MM, Breugem TI, Mykytyn AZ, et al. Human organoid systems reveal in vitro correlates of fitness for SARS-CoV-2 B.1.1.7. *bioRxiv*. 2021:2021.05.03.441080.
- [16] Mykytyn AZ, Rissmann M, Kok A, et al. Omicron BA.1 and BA.2 are antigenically distinct SARS-CoV-2 variants. *bioRxiv*. 2022:2022.02.23.481644.
- [17] Rockx B, Kuiken T, Herfst S, et al. Comparative pathogenesis of COVID-19, MERS, and SARS in a nonhuman primate model. *Science*. 2020 May 29;368(6494):1012–1015.
- [18] Sia SF, Yan LM, Chin AWH, et al. Pathogenesis and transmission of SARS-CoV-2 in golden hamsters. *Nature*. 2020 Jul;583(7818):834–838.
- [19] Abdullah F, Myers J, Basu D, et al. Decreased severity of disease during the first global omicron variant COVID-19 outbreak in a large hospital in Tshwane, South Africa. *Int J Infect Dis*. 2021 Dec 28;116:38–42.
- [20] Despres HW, Mills MG, Shirley DJ, et al. Measuring infectious SARS-CoV-2 in clinical samples reveals a higher viral titer: RNA ratio for Delta and Epsilon vs. Alpha variants. *Proc Natl Acad Sci U S A*. 2022 Feb 1;119(5):e2116518119.
- [21] Fall A, Eldesouki RE, Sachithanandham J, et al. A quick displacement of the SARS-CoV-2 variant delta with Omicron: unprecedented spike in COVID-19 cases associated with fewer admissions and comparable upper respiratory viral loads. *medRxiv*. 2022 Jan 28.
- [22] Yuan S, Ye Z-W, Liang R, et al. The SARS-CoV-2 Omicron (B.1.1.529) variant exhibits altered pathogenicity, transmissibility, and fitness in the golden Syrian hamster model. *bioRxiv*. 2022:2022.01.12.476031.
- [23] Haagmans BL, Noack D, Okba NMA, et al. SARS-CoV-2 neutralizing human antibodies protect against lower respiratory tract disease in a hamster model. *J Infect Dis*. 2021;223(12):2020–2028.
- [24] Mykytyn AZ, Breugem TI, Riesebosch S, et al. SARS-CoV-2 entry into human airway organoids is serine protease-mediated and facilitated by the multibasic cleavage site. *Elife*. 2021 Jan 4;10:e64508.
- [25] Lamers MM, Mykytyn AZ, Breugem TI, et al. Human airway cells prevent SARS-CoV-2 multibasic cleavage site cell culture adaptation. *Elife*. 2021 Apr 9;10:e66815.
- [26] Johnson BA, Xie X, Bailey AL, et al. Loss of furin cleavage site attenuates SARS-CoV-2 pathogenesis. *Nature*. 2021 Mar;591(7849):293–299.
- [27] Lau SY, Wang P, Mok BW, et al. Attenuated SARS-CoV-2 variants with deletions at the S1/S2 junction. *Emerg Microbes Infect*. 2020 Dec;9(1):837–842.
- [28] Meng B, Abdullahi A, Ferreira IATM, et al. Altered TMPRSS2 usage by SARS-CoV-2 Omicron impacts infectivity and fusogenicity. *Nature*. 2022 2022/03/01;603(7902):706–714.
- [29] Lamers MM, Mykytyn AZ, Breugem TI, et al. SARS-CoV-2 Omicron efficiently infects human airway, but not alveolar epithelium. *bioRxiv*. 2022:2022.01.19.476898.
- [30] Uraki R, Kiso M, Iida S, et al. Characterization and antiviral susceptibility of SARS-CoV-2 omicron/BA.2. *Nature*. 2022/05/16;2022.
- [31] Wei C, Shan KJ, Wang W, et al. Evidence for a mouse origin of the SARS-CoV-2 Omicron variant. *J Genet Genomics*. 2021 Dec;48(12):1111–1121.
- [32] Hansen F, Meade-White K, Clancy C, et al. SARS-CoV-2 reinfection prevents acute respiratory disease in Syrian hamsters but not replication in the upper respiratory tract. *Cell Rep*. 2022 Mar 15;38(11):110515.